

SURE-based Automatic Parameter Selection For ESPIRiT Calibration

Siddharth Iyer^{1,2,4}, Frank Ong¹, Kawin Setsompop², Mariya Doneva³, and Michael Lustig¹

¹Department of Electrical Engineering and Computer Science, University of California, Berkeley, California, 94720,
United States of America

²Athinoula A. Martinos Center for Biomedical Imaging, Department of Radiology, Massachusetts General Hospital,
Charlestown, Massachusetts, 02129, United States of America

³Philips Research Laboratories, Hamburg, Germany

⁴Department of Electrical Engineering and Computer Science, Massachusetts Institute of Technology, Cambridge,
Massachusetts, 02139, United States of America

Running head: SURE-Calibrated ESPIRiT.

Address correspondence to:

Michael Lustig
506 Cory Hall
University of California, Berkeley
Berkeley, CA 94720
United States of America
mlustig@eecs.berkeley.edu

This work was supported by NIH R01EB019241, NIH R01EB009690, NSF Graduate Fellowship, U24EB029240, R01HL136965, R01EB026136, NIH R01EB020613, R01 MH116173

Approximate word count: 200 (Abstract) 5000 (body)

Part of this work has been presented at the ISMRM Annual Conference 2016.

Published at *Magnetic Resonance in Medicine* as a Full Paper.

Abstract

Purpose: ESPIRiT is a parallel imaging method that estimates coil sensitivity maps from the auto-calibration region (ACS). This requires choosing several parameters for the optimal map estimation. While fairly robust to these parameter choices, occasionally, poor selection can result in reduced performance. The purpose of this work is to automatically select parameters in ESPIRiT for more robust and consistent performance across a variety of exams.

Methods: By viewing ESPIRiT as a denoiser, Stein’s unbiased risk estimate (SURE) is leveraged to automatically optimize parameter selection in a data-driven manner. The optimum parameters corresponding to the minimum true squared error, minimum SURE as derived from densely-sampled, high-resolution, non-accelerated data, and minimum SURE as derived from ACS are compared using simulation experiments. To avoid optimizing the rank of ESPIRiT’s auto-calibrating matrix (one of the parameters), a heuristic derived from SURE-based singular value thresholding is also proposed.

Results: Simulations show SURE derived from the densely-sampled, high-resolution, non-accelerated data to be an accurate estimator of the true mean squared error, enabling automatic parameter selection. The parameters that minimize SURE as derived from ACS correspond well to the optimal parameters. The soft-threshold heuristic improves computational efficiency while providing similar results to an exhaustive search. In-vivo experiments verify the reliability of this method.

Conclusion: Using SURE to determine ESPIRiT parameters allows for automatic parameter selections. In-vivo results are consistent with simulation and theoretical results.

Keywords: Parallel Imaging Calibration, *ESPIRiT*, *Stein’s Unbiased Risk Estimate*.

Introduction

Modern MRI leverages multiple receive coil arrays to perform parallel imaging (PI) for faster acquisition-time and improved signal to noise ratio (SNR). The high level mechanics of PI can be broken up into two steps: calibration and reconstruction. Calibration typically involves exploiting the data redundancy provided by the multiple receive channels to derive linear data consistency operators that define the subspace the signal is expected to live in. Reconstruction then enforces data consistency through these derived operators along with other priors to reconstruct the desired image.

Consider the two most common PI techniques, SENSE [1] and GRAPPA [2]. Both methods can be broken down into the two steps. SENSE is an image-domain method that uses an explicit calibration scan to derive explicit spatial coil sensitivity maps (CSM), which is then used as a spatial weighting operator during the reconstruction step. GRAPPA uses auto-calibration signal (ACS) lines or a separate calibration scan to derive convolution kernels in k-space that enforce data consistency.

In this work, the calibration of ESPIRiT [3] is studied. ESPIRiT is a method that bridges SENSE and GRAPPA by using ACS to derive so called ESPIRiT maps that can be used in a SENSE-like reconstruction. In ESPIRiT, there are several user-set parameters in the calibration that determine the quality of the resulting ESPIRiT maps. These parameters are described in the theory section. While ESPIRiT is in general robust to variation in these parameters, occasionally, poor parameter choice can result in reduced PI performance like noise amplification or image attenuation. This is exemplified in Figure 1, where different parameter choices result in ESPIRiT maps with significant variations in terms of signal attenuation and noise amplification. This motivates the study of ESPIRiT parameter selection.

Since the quality of MRI reconstruction is often quantified in terms of Mean Squared Error (MSE), it is desirable to select parameters that result in ESPIRiT maps that would result in a minimum MSE reconstruction. However, calculating MSE as a function of the parameters is impossible without access to the true, under-lying noise-free image. To overcome this limitation, the parameter selection problem is reformulated into a denoising problem, where ESPIRiT is viewed as a linear denoiser of the calibration data. This formulation allows Stein’s Unbiased Risk Estimate (SURE) [4] to be used. SURE is a technique that calculates the expected MSE of a given denoiser, and has seen widespread applicability in the field of denoising [5, 6, 7, 8]. By calculating SURE as a function of ESPIRiT parameters, the expected MSE of the corresponding ESPIRiT maps can be calculated and used to determine the optimal ESPIRiT map in this expected MSE sense. Succinctly, SURE is used as a proxy to the underlying MSE for parameter optimization.

In order to calculate SURE for a given denoiser, it is required to calculate the divergence of the denoiser with respect to the acquired data [4, 9]. This is often very difficult for general denoising algorithms, resulting in the emergence of Monte-Carlo methods. In particular, Ramani et al. demonstrates how Monte-Carlo simulations can calculate the divergence term required by SURE for a general (possibly non-linear) denoiser and provides a black-box framework for denoiser parameter optimization [9]. This Monte-Carlo SURE-framework has seen successful application to parallel imaging. Weller et al. presents a SURE-based method of selecting regularization for k-space data-consistency linear operators (GRAPPA [2] and SPIRiT [10]) that optimizes the linear operator for reconstruction [11, 12].

However, as discussed by Ramani et al., the divergence of a linear denoising operator corresponds to the trace of the operator. Consequently, if it is feasible to calculate the trace, the exact SURE value is obtained while avoiding Monte-Carlo simulations. This work demonstrates that, when considering non-accelerated, densely-sampled, high-resolution data, the exact SURE value can be calculated as a function of ESPIRiT parameters. In this case, ESPIRiT decouples into image-domain pixel-wise operators for which the divergence can be calculated exactly to be the trace of said operators which can be calculated efficiently. This work then augments ESPIRiT with a projection onto ACS to construct an ACS denoiser, and calculates the exact SURE value for this approximate problem. It is seen that the parameters corresponding to the minimum SURE as derived from ACS correspond well to the optimal parameters derived from the minimum true squared error.

This allows for near-optimum parameter estimation while overcoming the need to perform Monte-Carlo simulations. That being said, it is expected that the Monte-Carlo methods will achieve similar results with a larger computational cost.

This work calculates SURE for ESPIRiT by partitioning the complex vector space into real and imaginary parts, and takes advantage of the Hermitian symmetric characteristics of the ESPIRiT operator for efficient calculation of the divergence term required by SURE. This is discussed in the Theory section and in the Appendix. By partitioning the vector space, the application of SURE to ESPIRiT in this work fits within the general linear denoiser framework presented by Ramani et al. [9].

Using SURE as a metric to quantitatively evaluate the performance of ESPIRiT parameters is desirable as it avoids adding further model complexity and regularization to ESPIRiT. This is in contrast to methods where regularization, additional iterations and other techniques are incorporated into the model to build-in noise robustness while performing calibration [13, 14, 15, 16].

While this work focuses on ESPIRiT, the main theme of this work is to demonstrate how the quantitative

comparison of the denoising efficacy of a PI operator can be used to perform optimal PI calibration. The field of PI is extensive with many novel methods designed to fill different requirements and applications. The proposed reformulation of the calibration step can be applied to many other novel PI methods as well. For example, the matrix low-rank optimization in Parallel-LORAKS [17] can be reformulated into a matrix denoising problem, where SURE can be used to find the optimal soft threshold to denoise the matrix [18]. The encoding matrix presented in Joint-SENSE [19] will also benefit from the application of SURE. SURE can be calculated as a function of the polynomial coefficients used in Joint-SENSE to approximate CSM to determine which derived CSM best denoises ACS data. For GRAPPA based methods like iterative GRAPPA [20], a Tikhonov parameter can be introduced into the least squared fitting procedure, and this can be optimized over with SURE. However, this reformulation is unlikely to benefit techniques involving non-linear functions acting on noise as the noise model assumed by SURE no longer holds. For example, [21, 22] involve non-linear mapping of data, and [14, 15] explicitly rely on CS for noise robustness; both of which change the noise model assumed by SURE.

Additionally, while this work presents the concept of ESPIRiT calibration based on its denoising efficacy, there have been numerous works done on using SURE in the regime of regularization selection for MRI reconstruction. For example, Ramani et al. presented a framework for tuning non-linear reconstructions based on their respective Jacobians evaluated on acquired data [23]; and Marin et al. presented a parameterized wavelet-based estimator that uses SURE to determine the optimal parameters for reconstruction [24]. These works focus on selecting optimal regularization parameters for reconstruction, and often include a data-consistency term in the reconstruction formulation. Consequently, the SURE-based calibration in this work should work synergistically with these methods as it is expected to improve the performance of the data-consistency operator.

Finally, one of the parameters in ESPIRiT determines the rank of a block Hankel structured auto-calibration matrix. This work first demonstrates how SURE can be used to optimize for the same, then presents a singular value soft-thresholding heuristic derived from the SURE-based low rank matrix approximation theory developed by Candès et al. [18] to reduce computational overhead. The heuristic uses the SURE-optimal soft threshold derived by Candès et al. to weight the singular vectors of the auto-calibration matrix. This is seen to provide similar results to an exhaustive rank search while significantly reducing computational burden. The details of this heuristic is discussed in the sections below.

It should be explicitly noted that this work assumes that noise is additive, complex normal noise that is not correlated. If there is noise correlation between channels, the data should be whitened using noise characteristics derived from either the data itself or an explicit noise acquisition.

Theory

ESPIRiT

ESPIRiT is a technique that combines the data-based calibration advantages of GRAPPA to derive SENSE-like relative CSM. These CSM are derived from the null-space of the auto-calibration matrix, which is formed by sweeping a kernel through the calibration region (as depicted in Figure 2). The following provides a brief overview of ESPIRiT, with emphasis on the parameters that need to be tuned. For more detail about ESPIRiT and comparison to other PI methods, please refer to [3].

Let A be the auto-calibration matrix, $V_{||}$ be a matrix consisting of the right singular vectors of A corresponding to the dominant singular values of A , V_{\perp} be a matrix consisting of the remaining singular vectors that span the null space of A , U be a matrix consisting of the left singular vectors of A and Σ be a diagonal matrix consisting of the singular values of A in descending magnitude order. Then, by taking the singular value decomposition,

$$A = U\Sigma V^* \text{ with } V = \begin{bmatrix} V_{||} & V_{\perp} \end{bmatrix}. \quad (1)$$

Let y be the noise-free, fully-sampled, underlying multi-channel k-space data (at the sampling locations). Let R_r be an operator that extracts a block from y around the k-space position r (including r itself) across all the channels. Since the signal y should be orthogonal to the null-space of A , the following normal equations are derived:

$$\left(\sum_r R_r^* V_{\perp} V_{\perp}^* R_r \right) y = 0 \quad (2a)$$

$$\left(\sum_r R_r^* \left(I - V_{||} V_{||}^* \right) R_r \right) y = 0 \quad (2b)$$

$$\underbrace{\left(\sum_r R_r^* R_r \right)^{-1} \left(\sum_r R_r^* \left(V_{||} V_{||}^* \right) R_r \right)}_{\mathcal{W}} y = y \quad (2c)$$

$(\sum_r R_r^* R_r)^{-1}$ effectively scales each channel by a scalar that is the inverse of the number of k-space elements selected by R_r . Thus, \mathcal{W} is a convolution with a matrix-valued kernel where the matrix operates on the channel dimension. This convolution operator is decoupled into pixel-wise operations along the channel dimension in the image domain. In other words, let x be the true multi-channel image data such that $y = Fx$ where F is the unitary Fourier transform operator. Equation (2c) becomes,

$$\underbrace{(F^* \mathcal{W} F)}_{\mathcal{G}} x = x, \quad (3)$$

where \mathcal{G} is defined to be $F^*\mathcal{W}F$. Particularly, since \mathcal{G} is decoupled into pixel-wise operators, it suffices to look at the effect of \mathcal{G} on a particular image pixel with index q .

$$\mathcal{G}(q)x(q) = x(q) \quad (4)$$

$x(q)$ is a vector of dimension equal to the number of CSM. Let the source image be m and let S be the vector constructed from stacking the coil sensitivities of the different channels. The SENSE model states,

$$x(q) = S(q)m(q) \quad (5)$$

$m(q)$ is a scalar and $S(q)$ is a vector of dimension equal to the number of coil-sensitivity maps. Applying this to (4),

$$\mathcal{G}(q)S(q)m(q) = S(q)m(q) \quad (6)$$

If $m(q) \neq 0$, the following eigenvalue-eigenvector condition is derived:

$$\mathcal{G}(q)S(q) = 1 \cdot S(q) \quad (7)$$

Thus sensitivity maps, in the ideal case, are eigenvectors of \mathcal{G} with eigenvalues one, with the other eigenvectors of \mathcal{G} having eigenvalues much smaller than one. This comes from observing that \mathcal{W} is an average of projections and is consequently positive semi-definite with eigenvalues smaller or equal to one. In practice, due to data-inconsistencies (like noise), the observed eigenvalues of the eigenvector maps are very close to (but not exactly) one. This motivates defining an approximate “ ≈ 1 ” condition where the eigenvalues that would be 1 in the ideal case but are instead close to one. The eigenvalue decomposition of \mathcal{G} is taken and the eigenvector corresponding to eigenvalue “ ≈ 1 ” are considered to be ESPIRiT maps.

In some cases, multiple eigenvalues “ ≈ 1 ” appear such as when the calibration region supports a field-of-view smaller than the object which results in multiple sensitivity values at a pixel location due to aliasing [3]. This motivates using more than one set of these eigenvector maps to better capture the desired signal.

Parameter choices in ESPIRiT

There are three parameters in the ESPIRiT calibration. The first is the size of the window, or kernel, that is swept through the ACS to construct the auto-calibration matrix A ; the second is the size of the signal subspace used to partition $V_{||}$ from V_{\perp} ; and the third is the threshold, above which eigenvalues are considered “ ≈ 1 ”. These parameters are denoted as the kernel size (k), the subspace size (w) and the eigenvalue crop threshold (c), respectively.

Let n_c be the number of channels. For 2D data, a kernel size (k) would imply that window of dimensions ($k \times k \times n_c$) is swept through the calibration region to construct the rows of the auto-calibration matrix A . Consequently, $V_{||}$ and V_{\perp} together span a linear space of dimension ($k \cdot k \cdot n_c$), and the rank of $V_{||}$ can vary from 0 to ($k \cdot k \cdot n_c$). The chosen rank of $V_{||}$ is the subspace size (w) and is measured in Window Normalized Singular Values Number (WNSVN). This normalizes the rank by the kernel spatial dimensions and thus (w) is in the range from 0 to n_c . A subspace size of (w) implies $V_{||}$ consists of $w \cdot k^2$ orthogonal vectors. Finally, the eigenvalue crop threshold (c) determines the pixel positions (q) where the eigenvectors of operator $\mathcal{G}(q)$ are well defined, which corresponds to pixels positions (q) within the object. A too high threshold would result in direct attenuation of the signal, and too small a threshold would allow eigenvectors of operator $\mathcal{G}(q)$ from positions that are not well defined in terms of (7), which in turn allows in signal that is not necessarily from the object, such as noise. The feasible values of the eigenvalue crop threshold (c) are from 0 to 1, with realistic values residing in the range from 0.7 to 0.95. The rank of $V_{||}$ also represents a similar trade-off. Since the same under-lying data is observed through multiple receive channels, the auto-calibration matrix A is expected to be low-rank, but this is often not the case due to noise and other data inconsistencies. Since the ESPIRiT operator is derived from $V_{||}$, too large a subspace size implies that the ESPIRiT operator captures these inconsistencies within its range space while too small a subspace size yields an operator with insufficient information to properly describe the underlying signal. In the latter case, a projection onto the operator's range space will result in some signal loss. Lastly, the kernel size (k) of ESPIRiT determines the smoothness of the resulting ESPIRiT maps, where a smaller kernel results in smoother CSM. However, a too small kernel size may result in a calibration matrix A whose $V_{||}$ does not contain sufficient information to create the SENSE-like operator.

While ESPIRiT is fairly robust to these parameter choices, there is variability in map quality (such as how well the maps capture the field of view of the object) and choosing parameters that result in optimal reconstruction is desirable. Figure 1 exemplifies the variability in ESPIRiT maps when varying the subspace size (w) and eigenvalue crop threshold (c) for a fixed kernel size (k).

In order to develop a robust, data-driven method of automatic parameter selection, Stein's unbiased risk estimate (SURE) is explored as a metric to select parameters that are optimal in an expected mean squared error sense.

Stein's unbiased risk estimate

Stein's unbiased risk estimate is a data-driven method of calculating the expected mean squared error of an estimator in the presence of zero-mean additive Gaussian noise, given that the estimator is differentiable with respect to the data almost everywhere [4]. The SURE expression for a Hermitian symmetric operator is presented and then extended to ESPIRiT.

Let $x \in \mathbb{C}^m$ be the ground truth to be estimated; n be zero-mean, additive, Gaussian complex noise with standard deviation σ ; and $x_{\text{acq}} = x + n$ be the acquired data. Let $\mathbf{P}_\theta \in \mathbb{C}^{m \times m}$ be a Hermitian symmetric linear operator, parameterized by θ , that is an estimator of x for x_{acq} .

This work assumes that the noise is additive, normal noise that is not correlated. If there is noise correlation between channels, the data should be pre-whitened using noise characteristics derived either from the data itself or from an explicit noise measurement.

Let $\mathbb{E}\{\cdot\}$ denote the expected value operation. Partitioning the complex vector space into real and imaginary parts and noting that the divergence of a linear operator is the trace of the linear operator (steps described in the appendix), Stein's first theorem [4] implies:

$$\mathbb{E} \left\{ \|\mathbf{P}_\theta x_{\text{acq}} - x\|_2^2 \right\} = \mathbb{E} \{ \text{SURE}_{\mathbf{P}_\theta}(x_{\text{acq}}) \} \quad (8a)$$

$$\begin{aligned} \text{SURE}_{\mathbf{P}_\theta}(x_{\text{acq}}) &= -m\sigma^2 + \|(\mathbf{P}_\theta - I)x_{\text{acq}}\|_2^2 + 2\sigma^2 [\text{div}_{x_{\text{acq}}}(\mathbf{P}_\theta)](x_{\text{acq}}) \\ &= -m\sigma^2 + \|(\mathbf{P}_\theta - I)x_{\text{acq}}\|_2^2 + 2\sigma^2 \text{trace}(\mathbf{P}_\theta) \end{aligned} \quad (8b)$$

Particularly, note that Equation (8b) is independent of x , and only depends on the acquired data x_{acq} . Thus SURE can be used as a surrogate for the expected mean squared error to find the optimal parameters θ^* .

SURE with ESPIRiT

The main concepts will first be illustrated through a non-accelerated, densely-sampled, high-resolution case where the requirement of zero-mean additive normal noise is satisfied. In this case, there will be no noise-amplification due to data interpolation and the efficacy of the ESPIRiT operator is tied to the quality of the denoising it performs. This will later extend to the case when the densely-sampled region is restricted to the low-resolution ACS signal.

To quantify denoising, first define an ESPIRiT projection operator, which denoises the acquired data

using a projection onto the ESPIRiT maps. An illustration is provided in Figure 2f.

Let x_{acq} denote the acquired multi-channel images obtained from applying a Discrete Fourier transform on the non-accelerated, densely-sampled, high-resolution acquired k-space. Let n_c be the number of coils. Let $S^i(q)$ be the i^{th} eigenvector of $\mathcal{G}(q)$ with eigenvalue $\lambda_i(q)$. $S^i(q)$ is a vector of dimension n_c and has unit norm. Since \mathcal{G} , and consequently $\mathcal{G}(q)$, is Hermitian symmetric, the eigenvectors $S^i(q)$ will be orthonormal to each other. The ESPIRiT projection operator at pixel position q , which will be denoted as $P(q)$, is defined as:

$$\mathbf{P}(q) = \begin{bmatrix} | & & | \\ S^1(q) & \dots & S^{n_c}(q) \\ | & & | \end{bmatrix} \begin{bmatrix} | & & | \\ S^1(q) & \dots & S^{n_c}(q) \\ | & & | \end{bmatrix}^* \quad (9)$$

The aggregate ESPIRiT projection operator \mathbf{P} can be represented by stacking the pixel-wise operators diagonally:

$$\mathbf{P} = \begin{bmatrix} \mathbf{P}(1) & \dots & 0 \\ \vdots & \ddots & \vdots \\ 0 & \dots & \mathbf{P}(N) \end{bmatrix} \quad \text{where } N \text{ is the number of image pixels.} \quad (10)$$

The range space of the ESPIRiT projection operator describes the linear subspace the desired signal is expected to reside in. Projecting onto this subspace is expected to remove undesirable signal such as additive, white, Gaussian noise that contaminates MRI data. This interpretation of ESPIRiT as a denoiser allows for the application of SURE.

Let \mathbf{P}_θ be the projection operator derived from a particular ESPIRiT parameter set $\theta = (k, w, c)$. Define x as the densely-sampled, high-resolution, noise-less, multi-channel images; n as additive, complex normal noise of standard deviation σ ; $x_{acq} = x + n$ as the acquired coil images; and I as the identity operator. In this densely-sampled, high-resolution case, finding the optimal projection operator is reduced to finding the optimum θ^* that results in a projection operator \mathbf{P}_{θ^*} that best denoises the input data x_{acq} . That is to say,

$$\theta^* = \arg \min_{\theta} \|x - \mathbf{P}_\theta x_{acq}\|_2^2 \quad (11)$$

Since ESPIRiT is a pixel-wise linear projection operator in the image domain, the divergence contributed by a single pixel $x(q)$ is the trace of the linear operator affecting that pixel (denoted $\mathbf{P}_\theta(q)$) (described in the appendix). Thus, the SURE value of \mathbf{P}_θ can be calculated by summing over all pixel positions q .

$$SURE_\theta(v) = \sum_q \left[-n_c \sigma^2 + \|(\mathbf{P}_\theta(q) - I) x_{acq}(q)\|_2^2 + 2\sigma^2 \text{trace } \mathbf{P}_\theta(q) \right] \quad (12)$$

Equation (12) can then be used as a surrogate for (11).

$$\theta^* = \arg \min_{\theta} \|\mathbf{P}_\theta x_{acq} - x\|_2^2 \approx \arg \min_{\theta} SURE_\theta(x_{acq}) \quad (13)$$

Since the trace of AB is equal to the trace of BA for any matrix A and B , and since $S^i(q)$ are orthonormal to each other, the trace of \mathbf{P}_θ can be efficiently calculated by permuting the matrices in Equation (9).

$$\text{trace } \mathbf{P}_\theta = \sum_q \sum_i \|S^i(q)\|^2 \quad (14)$$

Thus, in the above case, it is possible to search through values of θ to determine the optimal projection operator \mathbf{P}_θ for calibration. Equation (13) is used as a basis to optimize for the ESPIRiT projection operator. A variant of (13) is presented in the following for the case in which the densely sampled region is limited to only the ACS data.

Accelerated case with the auto-calibration signal

In order to accelerate PI scans while still being auto-calibrating, the ESPIRiT operator is estimated from only the low-resolution, densely sampled ACS data. This is accomplished by incorporating a Fourier sampling operator into the projection operator \mathbf{P} and enforcing data consistency within the ACS data in k-space.

Define R to be the operator that outputs an ACS region from densely-sampled k-space. Let a new, augmented projection operator \mathbf{P}_θ^R be defined as follows:

$$\mathbf{P}_\theta^R = RFSS^*F^*R^* \quad (15)$$

Let y be the noise-less, densely-sampled, low-resolution auto-calibration region in k-space; n be additive, zero-mean, complex normal noise of standard deviation σ ; and $y_{\text{acq}} = y + n$ be the acquired auto-calibration region. Then, interpreting (15) as a denoiser of ACS data yields the following SURE expression:

$$\text{SURE}_\theta(y) = \|(\mathbf{P}_\theta^R - I) y_{\text{acq}}\|_2^2 + 2\sigma^2 \text{trace } \mathbf{P}_\theta^R + C \quad (16)$$

C is some constant term that is ignored because it does not affect the minimum. Since the trace of a matrix does not depend on a basis and F^* is a change of basis, it follows that,

$$\text{trace } \mathbf{P}_\theta^R = \text{trace } RFSS^*F^*R^* = \text{trace } F^*RFSS^*F^*R^*F \quad (17)$$

Thus, the trace can be calculated efficiently in a manner similar to Equation (14).

$$\text{trace } \mathbf{P}_\theta^R = \sum_q \sum_i \|\underline{S}^i(q)\|^2 \text{ where } \underline{S} = F^*RFS \quad (18)$$

Note that the exact SURE value is calculated for a denoiser constructed by augmenting ESPIRiT with a projection onto ACS. Since this is a different denoising operator (compared to the previous densely-sampled,

high-resolution non-accelerated case), the SURE values calculated (via Equations (16) and (12)) will not necessarily match. That being said, the SURE values calculated by Equations (16) and (12) are exact for their respective denoisers.

The parameters (θ) obtained from minimizing Equations (12) and (16) often correspond in practice. With the assumption that the optimal ESPIRiT maps are derived from parameters that best denoise densely-sampled, high-resolution, non-accelerated data, near optimal parameter selection while being limited to ACS is achieved.

Enforcing consistency of ACS data and the corresponding SURE expression is seen to be a good representative of the performance of ESPIRiT maps. This allows different parameter sets to be searched through to obtain the ESPIRiT projection operator that results in near-optimal performance in the expected mean squared error sense even when restricted to ACS data.

Soft-threshold based weighting for subspace estimation

In practice, sweeping through different kernel sizes and signal subspace sizes (or the rank of A and $V_{||}$) is computationally intensive whereas sweeping through different thresholds to determine the eigenvalue crop threshold (c) is relatively quick. To aid viability, a heuristic that appropriately weights the right singular vectors based on singular value soft-thresholding as an alternative to sweeping through different rank values is presented.

Since the same underlying data is being observed through multiple channels, the auto-calibration matrix A is expected to be low rank. However, due to noise and other data inconsistencies present in the data, the observed auto-calibration matrix often has full rank. A low-rank matrix estimate of A is then constructed by hard thresholding the singular values of A . Ideally, it would be beneficial to use SURE to determine the optimal low-rank matrix estimate in the sense of “denoising” the matrix. However, this is difficult to do since a hard threshold is not weakly-differentiable. A common alternative is to soft-threshold the singular values.

Consider the singular value decomposition of A in its dyadic form.

$$A = \sum_i s_i u_i v_i^* \quad (19)$$

Here, u_i are the left singular vectors, v_i are the right singular vectors and s_i are the singular values. A soft-threshold low rank matrix estimate of A , which will be denoted as \hat{A} , is constructed by soft-thresholding

the singular values by threshold λ .

$$\hat{A} = \sum_i (s_i - \lambda)_+ u_i v_i^* \quad (20)$$

If A does not contain structured noise, Candès et al. showed that it is possible to use SURE to efficiently find the optimal λ in Equation (20), which will be denoted as λ^* [18]. However, since A is block-Hankel, it contains structured noise. That being said, in this work, the method derived by Candès et al. is applied directly to obtain an approximate λ^* . With more relaxed computational efficiency requirements, black-box Monte-Carlo methods may be utilized to estimate λ^* , such as the work by Ramani et al. [9]. If computational efficiency is a non-issue, it is possible to utilize Equations (12) and (16) to enumerate all possible ranks of matrix A to determine the optimal rank of A . This is demonstrated by Experiment (a) in the Theory section.

The goal of this heuristic is to avoid enumerating the rank of A by incorporating λ^* to form a weighted subspace estimate. To motivate weighting the singular vectors, consider the following. The subspace selection problem can be modeled by a hard threshold on the singular values using a threshold λ .

$$V_{||} = VW \text{ where } W \text{ is a diagonal weight matrix with } W_{ii} = \begin{cases} 1, & (s_i > \lambda) \\ 0, & \text{otherwise} \end{cases} \quad (21)$$

Instead, weight the singular vectors with its soft-threshold variant that is used in (20). Let this weighted subspace be $V_{||}^w$.

$$V_{||}^w = VW \text{ where } W \text{ is a diagonal weight matrix with } W_{ii} = \frac{(s_i - \lambda)_+}{s_i} \quad (22)$$

The parameter λ^* is calculated by Candès' SURE method in (22) to get a weighted subspace estimate $V_{||}^w$. This weighted subspace estimate is then used in Equation (2c) instead of $V_{||}$.

The ESPIRiT operators derived from $V_{||}^w$ retain the differentiability property utilized by Equations (12) and (16). Consequently, the exact SURE value as a function of the crop threshold can be calculated for ESPIRiT operators derived from $V_{||}^w$.

Methods

To verify the efficacy of the technique, exhaustive simulation experiments are conducted using MATLAB (MathWorks, Natick, MA) to compare the true squared error and the expected risk as calculated by SURE for ESPIRiT. The feasibility of the method is demonstrated by conducting in-vivo experiments using ESPIRiT. Additionally, the soft-threshold heuristic with an eigenvalue crop threshold search (using a method akin to line-search) is implemented in the Berkeley Advanced Reconstruction Toolbox (BART) [25].

Simulation Experiments

Fully-sampled, high-resolution data of the human brain were acquired on a 1.5T scanner (GE, Waukesha, WI) using an eight-channel coil for a subject (with IRB approval and informed consent obtained). Data were collected obtained using inversion-recovery prepared 3D RF-spoiled gradient-echo sequence with the following parameters: $TR/TE = 12.2/5.2\text{ ms}$, $TI = 450\text{ ms}$, $FA = 20^\circ$, $BW = 15\text{ kHz}$, and a matrix size of $256 \times 180 \times 230$ with 1 mm isotropic resolution. This was done to have a ground-truth to compare against and verify the accuracy of SURE as an estimator of the mean squared error. The 3D dataset was Fourier transformed along the readout direction and a slice along the readout dimension was taken. ESPIRiT maps were calculated from this slice and the projection of this slice onto the ESPIRiT maps was considered to be the true, underlying ground truth. The ground truth has dimensions $230 \times 180 \times 8$, where 8 is the number of channels, and an l_2 -norm of 8369.46. Additive complex k-space noise of standard deviation 4 was retrospectively added to the ground-truth and the result was considered to be the acquired data.

For different parameter values (θ), ESPIRiT maps were generated and the true squared error between the projection and the ground truth was calculated. This error was compared to the calculated SURE value. The soft-threshold based weighting heuristic was also tested by similarly varying kernel sizes and eigenvalue crop thresholds and comparing the true squared error to SURE. For all the previous cases, the SURE approximation when being restricted to low-resolution, densely-sampled ACS data was also calculated.

In Experiment (a), a fixed kernel size of 6 was used and the subspace size and eigenvalue crop thresholds were varied. For each subspace size and eigenvalue crop threshold, the true squared error, SURE value given high-resolution, densely sampled data, and the SURE value given low-resolution, densely-sampled ACS data were calculated. The latter curve was normalized by a constant to better compare the minimums of each of the curves.

In Experiment (b), a fixed kernel size of 6 was used along with the soft-threshold based subspace weighting heuristic. The true squared error, SURE value given high-resolution, densely sampled data, and the SURE value given low-resolution, densely-sampled ACS data was calculated as the crop threshold was varied. The latter curve was normalized by a constant to better compare the minimum of each of the curves.

In Experiment (c), the same three curves were calculated from varying the kernel size, subspace size and eigenvalue crop threshold parameters. The minima given a particular kernel size across the subspace thresholds and eigenvalue crop thresholds for that kernel size were taken. This experiment was conducted to test the dependence of ESPIRiT maps on the kernel size (k) assuming optimal subspace size and eigenvalue

crop threshold for that particular kernel size (k).

In Experiment (d), the same three curves were calculated from varying the kernel size and eigenvalue crop threshold parameters while using the soft-threshold based subspace weighting heuristic. The minima across the eigenvalue crop thresholds given a particular kernel size were taken. This experiment was conducted to test the dependence of ESPIRiT maps on the kernel size (k) assuming an optimal eigenvalue crop threshold for that particular kernel size (k).

In Experiment (e), a fixed kernel size of 6 was used along with the soft-threshold based subspace weighting heuristic, and the eigenvalue crop threshold was varied. For each eigenvalue crop threshold, the true squared error and corresponding g-factor maps are calculated. The maximum and average g-factor within the field of view of the desired object is used to demonstrate how ESPIRiT maps calibrated according to the minimum squared error can aid with accelerated acquisitions. The g-factor maps are calculated assuming equispaced 2×2 sub-sampling in the phase encode directions.

Experiments (a, b, c, d, e) used an ACS size of 24×24 .

In-Vivo Experiments

In Experiment (f), a 3D accelerated dataset was acquired on a 3T Achieva scanner (Philips, Best, The Netherlands) with IRB approval and informed consent obtained. The acquisition was a T_1 -weighted, TFE dataset acquired using Poisson disk under-sampling ($R \sim 2$) with 18×18 ACS lines using an 8-channel head coil. The k-space data were pre-whitened using scanner software based on noise measurement. A unitary inverse Fourier transform was taken along the readout direction and a slice was extracted. ESPIRiT calibration was performed on the dataset using parameters selected by the SURE-based method with the soft-threshold based weighting heuristic. A fixed kernel size of 6 is used along with the line-search like method for calculating the eigenvalue crop threshold. A PI+compressed sensing (CS) iterative reconstruction was performed with the SURE-calibrated ESPIRiT maps (with an l_1 regularization of 0.01 using a wavelet sparsity prior). The iterative reconstruction used BART.

In Experiment (g), one pre-whitened 3D dataset was acquired on a 3T Skyra scanner (Siemens Healthcare, Erlangen, Germany) with IRB approval and informed consent obtained. The acquisition was a high resolution, densely sampled T_2 -weighted, TSE dataset with no under-sampling. The data is coil compressed from 32 channels to 8 channels using geometric coil compression [26]. A unitary inverse Fourier transform was taken along the readout direction and a slice was extracted. The densely sampled data was retrospec-

tively under-sampled using a 2×2 Poisson disk sampling mask and a 2×2 equispaced sampling mask. ESPIRiT calibration was performed on the dataset using parameters selected by the SURE-based method with the soft-threshold based weighting heuristic. A fixed kernel size of 6 is used along with the line-search like method for calculating the eigenvalue crop threshold. PI+CS iterative reconstructions was performed with the SURE-calibrated ESPIRiT maps (with an l_1 regularization of 0.01 using a wavelet sparsity prior). These iterative reconstructions were implemented in BART.

In Experiment (h), the SURE-based parameter selection is applied to the same data used in the original ESPIRiT work [3] that demonstrated ESPIRiT’s robustness to aliasing due to the calibration region supporting a FOV smaller than the object. The same 2D spin-echo dataset ($TR/TE = 550/14ms$, $FA = 90^\circ$, $BW = 19kHz$, matrix size: 320×168 , slice thickness: $3mm$, 24 reference lines) with an FOV of $(200 \times 150)mm^2$, acquired at $1.5T$ using an 8-channel head coil is used. Additionally, the data is retrospectively under-sampled using an equi-spaced 2×2 sampling mask with an ACS size of 24×24 . The data was Fourier transformed to the image domain and noise variance was estimated from a corner of the image data that did not contain any desired signal. To determine the ESPIRiT maps, a fixed kernel size of 6 is used along with the soft-threshold based weighted subspace estimate. The eigenvalue crop threshold was calculated using the line-search like method. The resulting ESPIRiT map was then calculated to verify robustness to aliasing.

Characterization Experiments

Experiment (i): Using the same data as in Experiment (a), ESPIRiT maps are calculated as a function of calibration size (r) using the soft-weighting heuristic and MSE-optimal crop threshold. A calibration size of r implies $(r \times r)$ ACS lines. The resulting projection MSE is also calculated. This is to characterize the effect of the number of ACS lines in deriving optimal ESPIRiT maps.

Experiment (j) explores the possibility of using SURE for more finely-tuned parameterization by calibrating ESPIRiT maps on a slice-by-slice basis that is SURE-optimal per slice. This should allow for ESPIRiT’s parameters to vary as a function of the noise level per slice. This concept is applied to the T_2 -weighted dataset in Experiment (g), where the SURE-calibration uses the soft-weighting heuristic. Additionally, this experiment compares the SURE-optimal calibration to default calibration parameters present currently in BART.

Experiment (k): It is also worthwhile considering the effects of kernel size when using the soft-threshold

heuristic and the SURE-optimized crop threshold. ESPIRiT calibration is performed on the same dataset as in Experiment (a), and g-factor is calculated as a function of kernel size (k).

Results

Simulation Results

The simulation results of Experiments (a), (b), (c) and (d) are illustrated in Figure 3. In Experiments (a) and (b), it is seen that the true squared error calculated with the densely-sampled, high-resolution data and SURE correspond well. It is also seen that SURE as calculated from ACS data has a minimum close to the minimum of the true squared error. Additionally, the minimum true squared error of Experiment (b) is higher than the minimum true squared error of Experiment (a) by approximately 1.34%, demonstrating that the soft-threshold heuristic yields ESPIRiT maps that perform almost as well as the optimal EPSIRiT maps derived from enumerating through the rank of the auto-calibration matrix. With comparable MATLAB (MathWorks, Natick, MA) implementations, the exhaustive rank search and crop threshold search in Experiment (a) took days to complete while the exhaustive crop threshold search with the soft-threshold heuristic in Experiment (b) completed in a few hours on an Intel(R) Xeon(R) Gold 6138 CPU. In comparison, for Experiment (h), the soft-threshold heuristic and crop threshold search implemented in BART completes in 7.112 seconds on the same CPU. Thus significant computational gain is achieved with minimal performance penalty. Experiments (c) and (d) do not show perfect correspondence. However, the squared error in these cases are in the order of 10^5 , which is much smaller than Experiments (a) and (b), where the squared errors are in the order of 10^7 .

The simulation results of Experiment (e) is illustrated in Figure 4. Note how until Point B, a decrease in the squared error corresponds to better g-factor performance, while any increase in the crop threshold beyond Point B attenuates the signal. This experiment demonstrates that, even though a crop threshold value reflect in Point A is sufficient, there is g-factor performance to be gained through optimizing for the minimum squared error.

On simulated data that fits the model, it is seen that SURE as estimated from densely-sampled, high-resolution non-accelerated data is an accurate estimator of the squared error. Furthermore, restricting ourselves to ACS results in near-optimal parameter choice.

In-Vivo Results

The results of Experiments (f), (g) and (h) are depicted in Figures 5, 6 and 7, respectively. Figures 5 and 6 show how SURE allows ESPIRiT to tightly capture the field of view of the desired object without attenuating the signal. Experiment (h) demonstrates that SURE calibration allows ESPIRiT to retain its robustness to aliasing when the FOV is smaller than object, while still capturing tightly the field of view of the desired object.

Characterization Results

The result of Experiment (i) is illustrated in Figure 8. While a larger calibration size does result in a lower squared error, the advantage is in the order of 10^5 , which is much smaller than optimizing other parameters depicted in Figure 3, which are in the order of 10^7 .

The result of Experiment (j) is illustrated in Figure 9. While the SURE-based parameters derive ESPIRiT maps that tightly support the FOV of the desired signal for most slices and is an improvement over the default parameters, the spurious signal outside the human body due to eye-motion related artifacts in Slice 125 results in ESPIRiT maps that do not non-tightly wrap around the FOV of the desired signal for both cases.

Experiment (k): The g-factor performance of calibrated ESPIRiT maps as a function of kernel size can be seen in Figure 10. This suggests that, when using an 8-channel coil, g-factor performance is fairly stable as a function of kernel size.

Discussion

With respect to an exhaustive subspace rank and crop threshold search, SURE as estimated from densely-sampled, high-resolution, non-accelerated data corresponds well to the true squared error, yielding optimal parameter selection in this full-data case since SURE is used as a proxy to the true squared error. The parameters that minimize SURE estimated from ACS correspond well to the optimum parameters that minimize full-data SURE. With the assumption that the optimal ESPIRiT maps are derived from parameters that best denoise densely-sampled, high-resolution, non-accelerated data, the resulting parameter choices are optimal in an expected error sense.

The soft-threshold heuristic is seen to significantly ease computational burden while yielding ESPIRiT maps that perform similarly to the optimal maps derived from an exhaustive rank search.

Using SURE as a metric to determine ESPIRiT parameters results in consistent performance across different datasets. In practice, with the parameter ranges mentioned in the in-vivo experiments, the resulting parameter choices tend to optimize for SNR performance while causing no signal attenuation.

Motion during the scan presents a challenge for estimating accurate auto-calibrated CSM, and the presented SURE-based parameter optimization can not solve this issue. In case of motion, the SURE optimized parameters may lead to CSM that extend outside of the images object as depicted by the eye-motion related artifacts in Slice 125 of Figure 9. Since SURE tries to avoid data attenuation at all costs, the ESPIRiT maps calibrated at this slice do not tightly wrap around the FOV of the desired signal. This is in contrast to Slice 1 of Figure 9, where the lack of motion allows SURE and ESPIRiT to very finely calibrate its support about the FOV of the desired signal.

While the soft-threshold weighting heuristic and line-search based crop threshold search does help alleviate some of the computational burden, there will always be added cost. For Experiment (h), ESPIRiT on BART takes 0.416 seconds using BART’s default parameters, versus 7.112 seconds using the soft-weighting heuristic and line-search on an Intel(R) Xeon(R) Gold 6138 CPU. However, this method does offer a robust, data-consistent metric that can adapt to the noise level for denoising while avoiding signal attenuation.

For practical usage, we recommend a kernel size of 6 – 8 with the soft-threshold based weighted subspace heuristic and at least 24 ACS lines. With respect to the “soft” SENSE model described in [3], we recommend using two ESPIRiT maps. While SURE should help determine the number of ESPIRiT maps as well, it would contribute non-trivially to the computational burden for minimal gain. If it is known the ACS prescribed FOV is sufficient for the object, one set of ESPIRiT maps is usually sufficient.

Conclusion

Using SURE as a metric to determine parameters in ESPIRiT allows for automatic parameter selections. In-vivo results are consistent with simulation and theoretical results.

Data Availability Statement

The MATLAB (MathWorks, Natick, MA) code and data that support the findings of the Experiments ($a - e, i, k$), used to produce Figures 3, 4, 7, 8, and 10, are openly available in <https://github.com/mikgroup/auto-espirit> at DOI:10.5281/zenodo.3679377. The C code that support the findings of Experiments (f, g, j), used to produce Figures 5, 6 and 9, is openly available as a part of the BART Toolbox in <https://github.com/mrirecon/bart/> at DOI:10.5281/zenodo.3376744, reference [25].

References

- [1] Pruessmann KP, Weiger M, Scheidegger MB, Boesiger P et al. SENSE: Sensitivity Encoding for Fast MRI. *Magnetic Resonance in Medicine* 1999; 42:952–962.
- [2] Griswold MA, Jakob PM, Heidemann RM, Nittka M, Jellus V, Wang J, Kiefer B, Haase A. Generalized Autocalibrating Partially Parallel Acquisitions (GRAPPA). *Magnetic Resonance in Medicine* 2002; 47:1202–1210.
- [3] Uecker M, Lai P, Murphy MJ, Virtue P, Elad M, Pauly JM, Vasanawala SS, Lustig M. ESPIRiT - An Eigenvalue Approach to Autocalibrating Parallel MRI: Where SENSE Meets GRAPPA. *Magnetic Resonance in Medicine* 2014; 71:990–1001.
- [4] Stein CM. Estimation of the Mean of a Multivariate Normal Distribution. *The Annals of Statistics* 1981; pp. 1135–1151.
- [5] Luisier F, Blu T, Unser M. A New SURE Approach to Image Denoising: Interscale Orthonormal Wavelet Thresholding. *IEEE Transactions on Image Processing* 2007; 16:593–606.
- [6] Zhang XP, Desai MD. Adaptive Denoising Based on SURE Risk. *IEEE Signal Processing Letters* 1998; 5:265–267.
- [7] Blu T, Luisier F. The SURE-LET Approach to Image Denoising. *IEEE Transactions on Image Processing* 2007; 16:2778–2786.
- [8] Luisier F, Blu T. SURE-LET Multichannel Image Denoising: Interscale Orthonormal Wavelet Thresholding. *IEEE Transactions on Image Processing* 2008; 17:482–492.
- [9] Ramani S, Blu T, Unser M. Monte-Carlo SURE: A Black-box Optimization of Regularization Parameters for General Denoising Algorithms. *IEEE Transactions on Image Processing* 2008; 17:1540–1554.

- [10] Lustig M, Pauly JM. SPIRiT: Iterative Self-Consistent Parallel Imaging Reconstruction from Arbitrary K-Space. *Magnetic Resonance in Medicine* 2010; 64:457–471.
- [11] Weller DS, Ramani S, Nielsen JF, Fessler JA. SURE-based Parameter Selection for Parallel MRI Reconstruction using GRAPPA and Sparsity. *2013 IEEE 10th International Symposium on Biomedical Imaging* 2013; pp. 954–957.
- [12] Weller DS, Ramani S, Nielsen JF, Fessler JA. Monte Carlo SURE-based Parameter Selection for Parallel Magnetic Resonance Imaging Reconstruction. *Magnetic Resonance in Medicine* 2014; 71:1760–1770.
- [13] Xu L, Feng Y, Liu X, Kang L, Chen W. Robust GRAPPA Reconstruction using Sparse Multi-kernel Learning with Least Squares Support Vector Regression. *Magnetic Resonance Imaging* 2014; 32:91–101.
- [14] Majumdar A, Chaudhury K, Ward R. Calibrationless Parallel Magnetic Resonance Imaging: A Joint Sparsity Model. *Sensors* 2013; 13:16714–16735.
- [15] Jin KH, Lee D, Ye JC. A General Framework for Compressed Sensing and Parallel MRI using Annihilating Filter Based Low-rank Hankel Matrix. *IEEE Transactions on Computational Imaging* 2016; 2:480–495.
- [16] Park S, Park J. Adaptive Self-calibrating Iterative GRAPPA Reconstruction. *Magnetic Resonance in Medicine* 2012; 67:1721–1729.
- [17] Haldar JP, Zhuo J. P-LORAKS: Low-rank Modeling of Local k-space Neighborhoods with Parallel Imaging Data. *Magnetic Resonance in Medicine* 2016; 75:1499–1514.
- [18] Candes EJ, SingLong CA, Trzasko JD. Unbiased Risk Estimates for Singular Value Thresholding and Spectral Estimators. *IEEE Transactions on Signal Processing* 2013; 61:4643–4657.
- [19] Ying L, Sheng J. Joint Image Reconstruction and Sensitivity Estimation in SENSE (JSENSE). *Magnetic Resonance in Medicine* 2007; 57:1196–1202.
- [20] Zhao T, Hu X. Iterative GRAPPA (iGRAPPA) for Improved Parallel Imaging Reconstruction. *Magnetic Resonance in Medicine* 2008; 59:903–907.
- [21] Chang Y, Liang D, Ying L. Nonlinear GRAPPA: A Kernel Approach to Parallel MRI Reconstruction. *Magnetic Resonance in Medicine* 2012; 68:730–740.
- [22] Lyu J, Nakarmi U, Liang D, Sheng J, Ying L. KerNL: Kernel-based Nonlinear Approach to Parallel MRI Reconstruction. *IEEE Transactions on Medical Imaging* 2018; 38:312–321.

- [23] Ramani S, Liu Z, Rosen J, Nielsen JF, Fessler JA. Regularization Parameter Selection for Nonlinear Iterative Image Restoration and MRI Reconstruction using GCV and SURE-based Methods. IEEE Transactions on Image Processing 2012; 21:3659–3672.
- [24] Marin A, Chaux C, Pesquet JC, Ciuciu P. Image Reconstruction from Multiple Sensors using Stein’s Principle. Application to Parallel MRI. 2011 IEEE International Symposium on Biomedical Imaging 2011; pp. 465–468.
- [25] Uecker M, Ong F, Tamir JI, Bahri D, Virtue P, Cheng JY, Zhang T, Lustig M. Berkeley Advanced Reconstruction Toolbox. Proc. Intl. Soc. Mag. Reson. Med 2015; 23:2486.
- [26] Zhang T, Pauly JM, Vasanawala SS, Lustig M. Coil Compression for Accelerated Imaging with Cartesian Sampling. Magnetic Resonance in Medicine 2013; 69:571–582.
- [27] Axler S, “Linear Algebra Done Right (Undergraduate Texts in Mathematics)”. Springer, 2016.

Appendix

Divergence of a Linear Operator (Used in Equations (8b) and (12))

Consider arbitrary $x \in \mathbb{C}^m$, $A \in \mathbb{C}^{m \times m}$ and let $f(x) = Ax$.

$$f(x) = \begin{bmatrix} A_{11} & \dots & A_{1m} \\ \vdots & \ddots & \vdots \\ A_{m1} & \dots & A_{mm} \end{bmatrix} \begin{bmatrix} x_1 \\ \vdots \\ x_m \end{bmatrix} \quad (23)$$

Succinctly,

$$f_i(x) = \sum_{j=1}^m A_{ij}x_j \quad (24)$$

Thus,

$$\begin{aligned} [\operatorname{div}_x f](x) &= \sum_{i=1}^m \left[\frac{\partial}{\partial x_i} f_i \right](x) \\ &= \sum_{i=1}^m [A_{ii}](x) \\ &= \operatorname{trace}(A) \end{aligned} \quad (25)$$

Derivation of Equation (8)

Let $x \in \mathbb{C}^m$ be the true, underlying data; n be zero-mean, additive, Gaussian, complex noise with the real and imaginary standard deviations of $\frac{\sigma}{\sqrt{2}}$ each; and $x_{\text{acq}} = x + n$ be acquired data. Let \mathbf{P} be the Hermitian symmetric projection operator.

Partition the complex vector space into real and imaginary parts to reduce this problem to the real case. Let x_R denote the partitioned form of x , \mathbf{P}_R denote the partitioned form of \mathbf{P} and so on. Then,

$$x_R = [\text{Re}(x), \text{Im}(x)]^T, x_{\text{acq}R} = [\text{Re}(x_{\text{acq}}), \text{Im}(x_{\text{acq}})]^T, \mathbf{P}_R = \begin{bmatrix} \text{Re}(\mathbf{P}) & -\text{Im}(\mathbf{P}) \\ \text{Im}(\mathbf{P}) & \text{Re}(\mathbf{P}) \end{bmatrix} \text{ etc.} \quad (26)$$

This partitioning allows the use [4] directly. Observe that the noise variance in the partitioned case is now $\frac{\sigma^2}{2}$.

$$\begin{aligned} \text{SURE}_{\mathbf{P}}(x_{\text{acq}}) &= -2m\frac{\sigma^2}{2} + \|(\mathbf{P} - I)x_{\text{acq}}\|_2^2 + 2\frac{\sigma^2}{2}\text{trace}(\mathbf{P}_R) \\ &= -m\sigma^2 + \|(\mathbf{P} - I)x_{\text{acq}}\|_2^2 + 2\sigma^2\text{trace}(\mathbf{P}) \end{aligned} \quad (27)$$

Using the fact that the eigenvalues of \mathbf{P} are real (since \mathbf{P} is Hermitian symmetric) and that the trace of a matrix is independent from basis of representation [27], it follows:

$$\text{trace}(\mathbf{P}_R) = 2\text{trace}(\mathbf{P}) \quad (28)$$

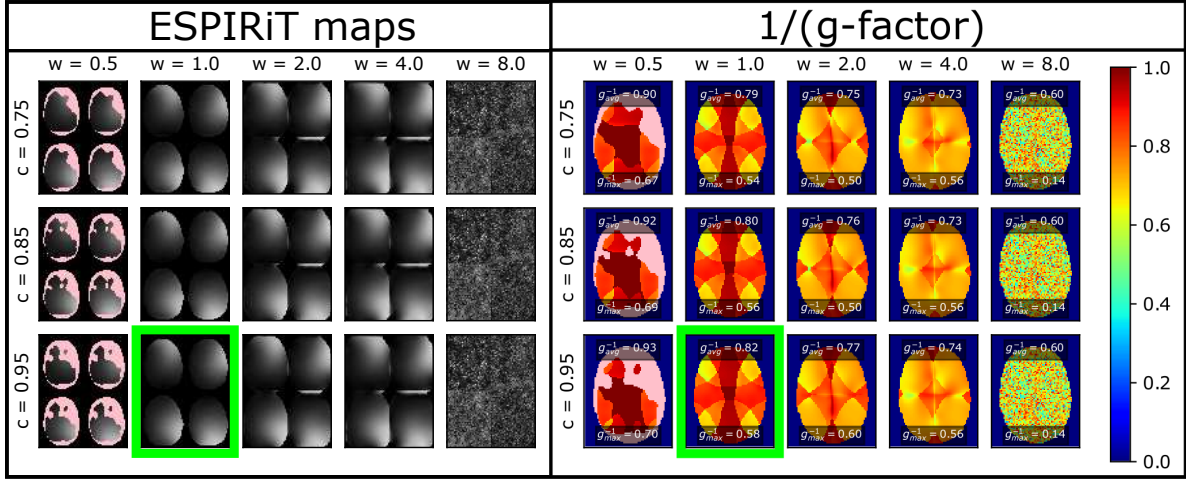
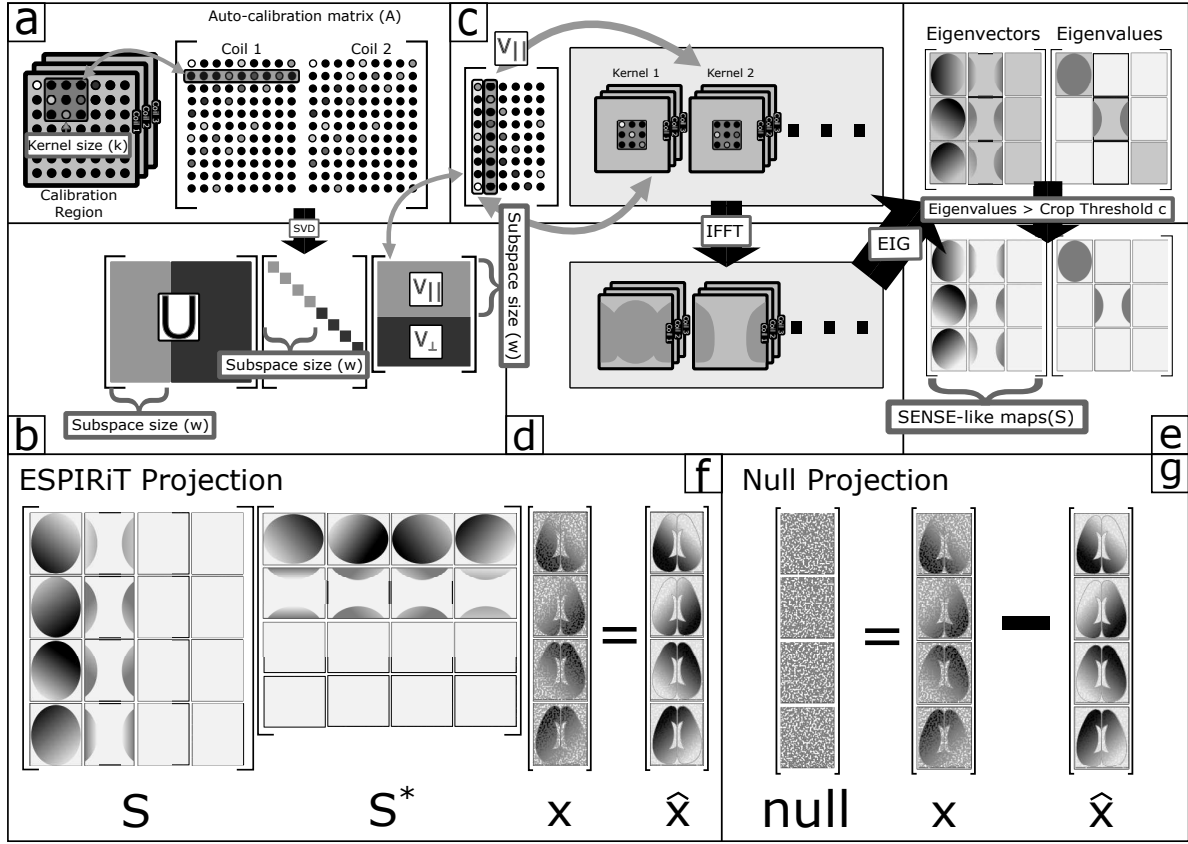


Figure 1: Variability in ESPIRiT maps is exemplified by varying the signal subspace size (w) in WNSVN and eigenvalue crop threshold (c). These parameters are explained in the theory section. The mean g-factor g_{avg} and maximum g-factor g_{max} within the field of view of the desired object is used to quantify the performance of the ESPIRiT maps. $1/g_{avg}$ and $1/g_{max}$ are listed at top and bottom of the g-factor maps respectively. The g-factor is calculated assuming equispaced 2×2 sub-sampling in the phase encode directions. ESPIRiT maps that do not attenuate signal but have a high $1/g_{avg}$ and $1/g_{max}$ are desirable. Light pink mark regions of signal attenuation. In this figure, the best example is marked with a green box.



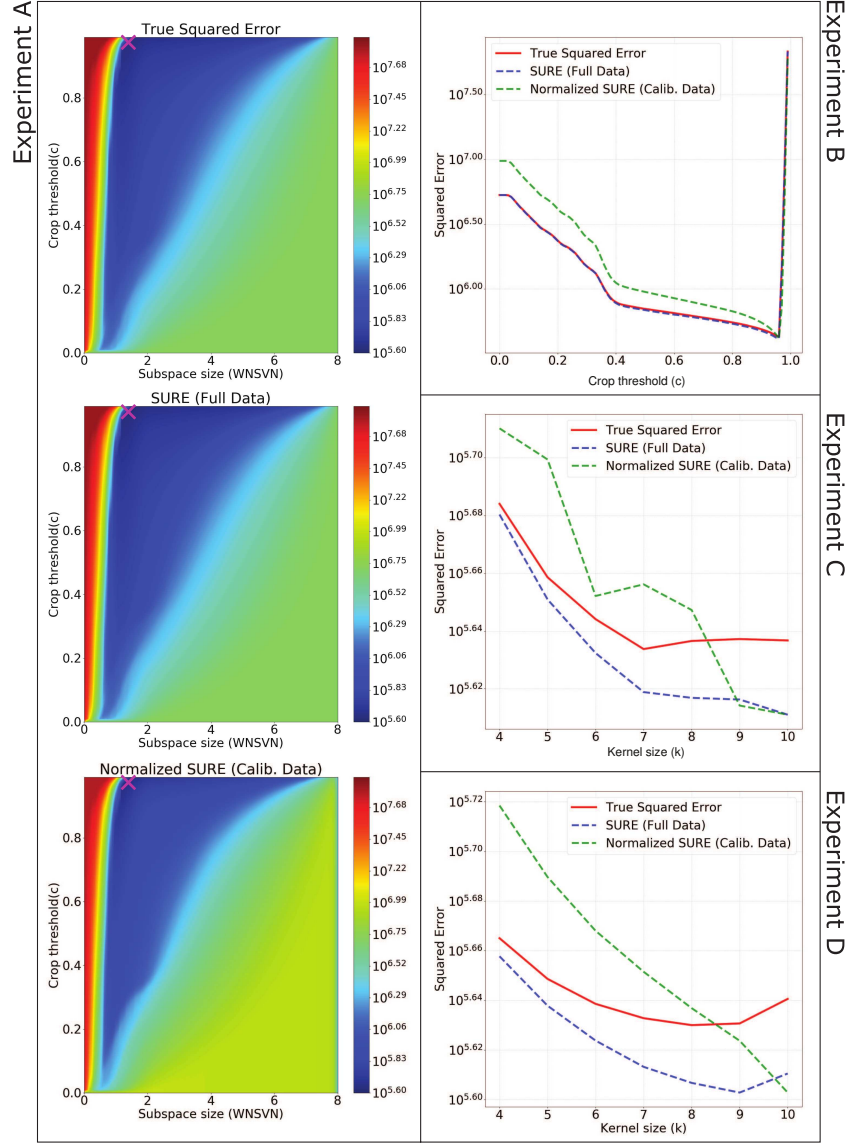


Figure 3: Experiment (a): with a fixed kernel size of 6, the true squared error, SURE given densely-sampled, high-resolution data and normalized SURE given ACS data is calculated as a function of subspace size and eigenvalue crop threshold. The purple crosses show the locations of the respective minimum values. Experiment (b): with a fixed kernel size of 6 along with the soft-threshold based subspace weighting heuristic, the true squared error, SURE given densely-sampled, high-resolution data and normalized SURE given ACS data is calculated as a function of the eigenvalue crop threshold. Experiment (c): True squared error, SURE given densely-sampled, high-resolution data and normalized SURE given ACS data is calculated as kernel size, subspace size and eigenvalue crop threshold parameters are varied. The minimum given a particular kernel size is taken. Experiment (d) is similar to Experiment (c), except that instead of calculating the optimal subspace size given the kernel size, the soft-threshold based subspace weighting heuristic is used.

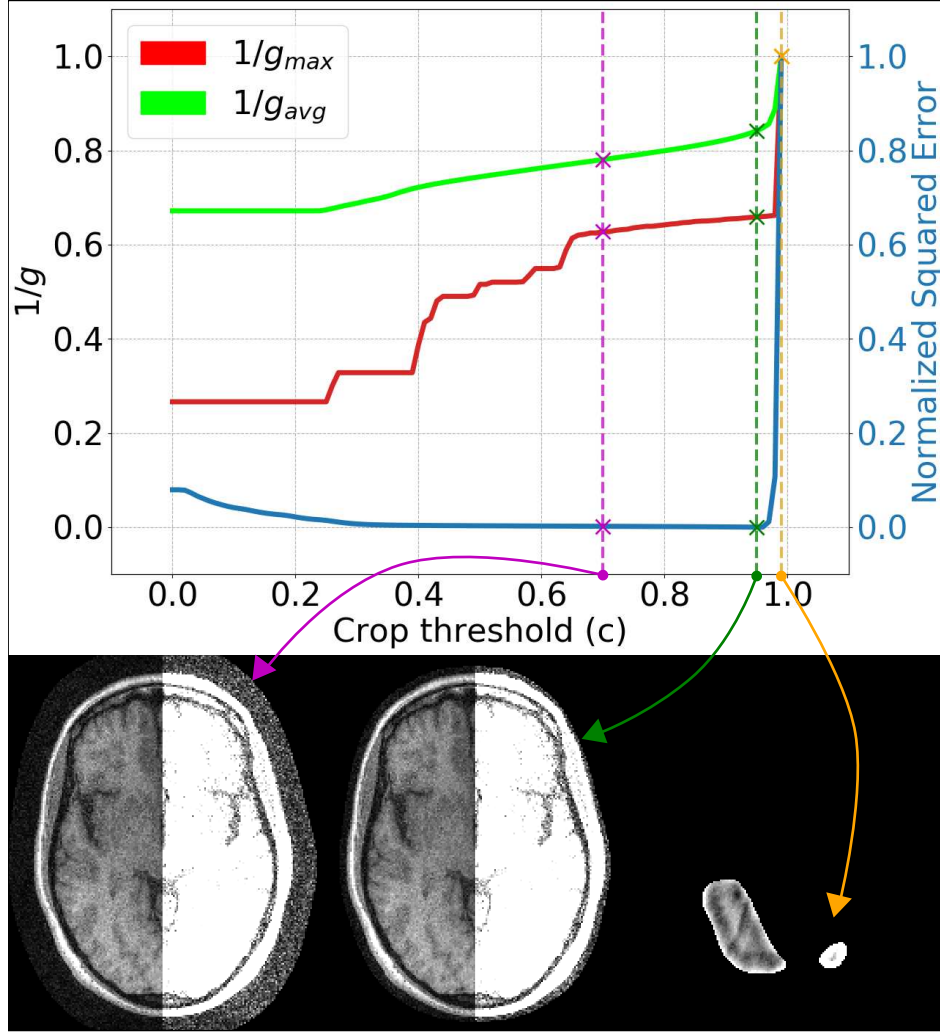


Figure 4: This figure shows how g-factor performance varies as a function of the Crop Threshold (c) when using the soft-weighting heuristic. The g-factor was calculated for voxels within the field of view of the brain using the same 2×2 equi-spaced sampling pattern described in Figure 1. Note that for all values of (c) to the left of the green line (marked B), an increase in (c) results in a decrease in squared error as well as better g-factor performance. However, for values of (c) to the right of B , the resulting maps attenuate the desired signal. This is reflected by the increase in squared error. The purple line A reflects a safe value of the crop threshold, B reflects the optimal value in terms of minimum squared error and C represents the best g-factor but at the cost of a lot of signal attenuation. The optimality of B is also reflected in how well the field of view of the desired signal is captured. Half of the image's contrast has been enhanced to illustrate this point.

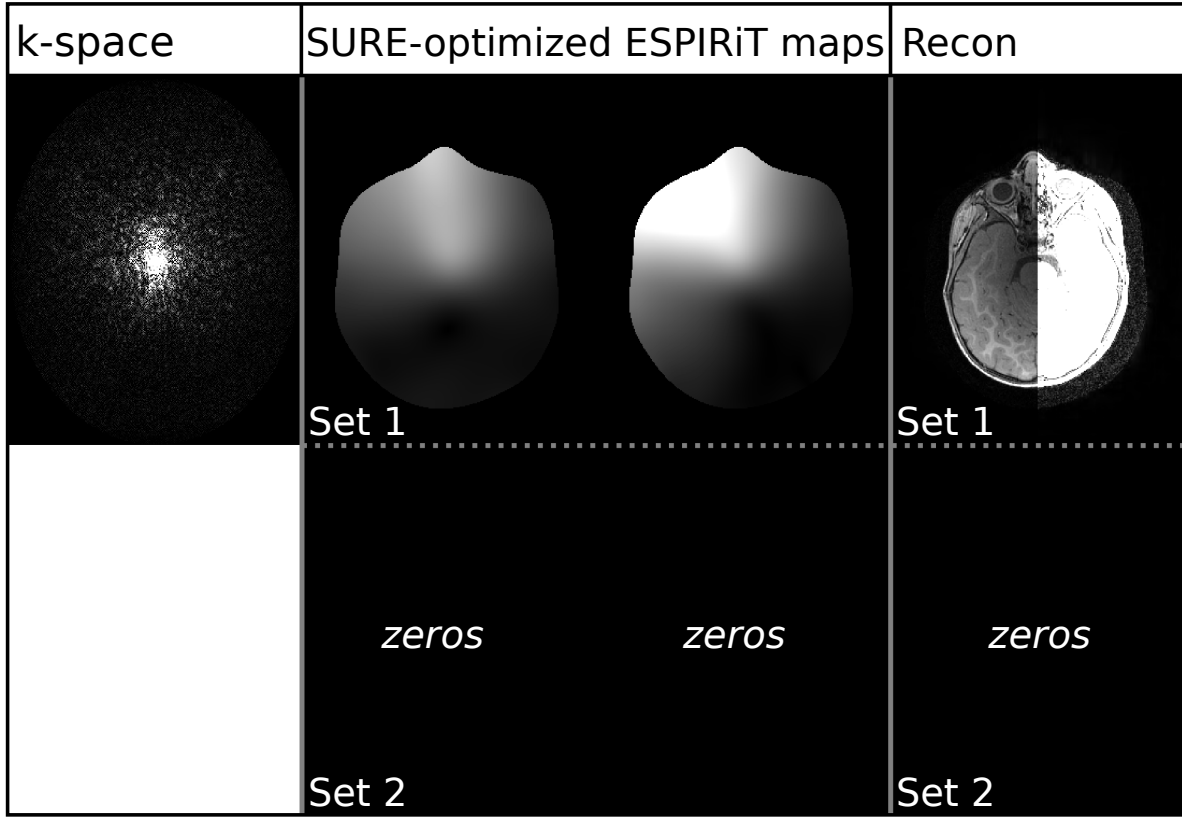


Figure 5: Experiment (f): This figure demonstrates the application of SURE to calibrate ESPIRiT maps on a T_1 -weighted acquisition where roughly 50% of the total phase encode points are acquired, which included an ACS size of 18×18 . Half of the image’s contrast has been enhanced to illustrate how well the field of view of the desired object has been captured. “Set 1” and “Set 2” refers the “soft” SENSE model, where multiple ESPIRiT maps may satisfy the “ ≈ 1 ” eigenvalue condition. 2 of the 8 calibrated ESPIRiT maps are depicted in this figure for brevity.

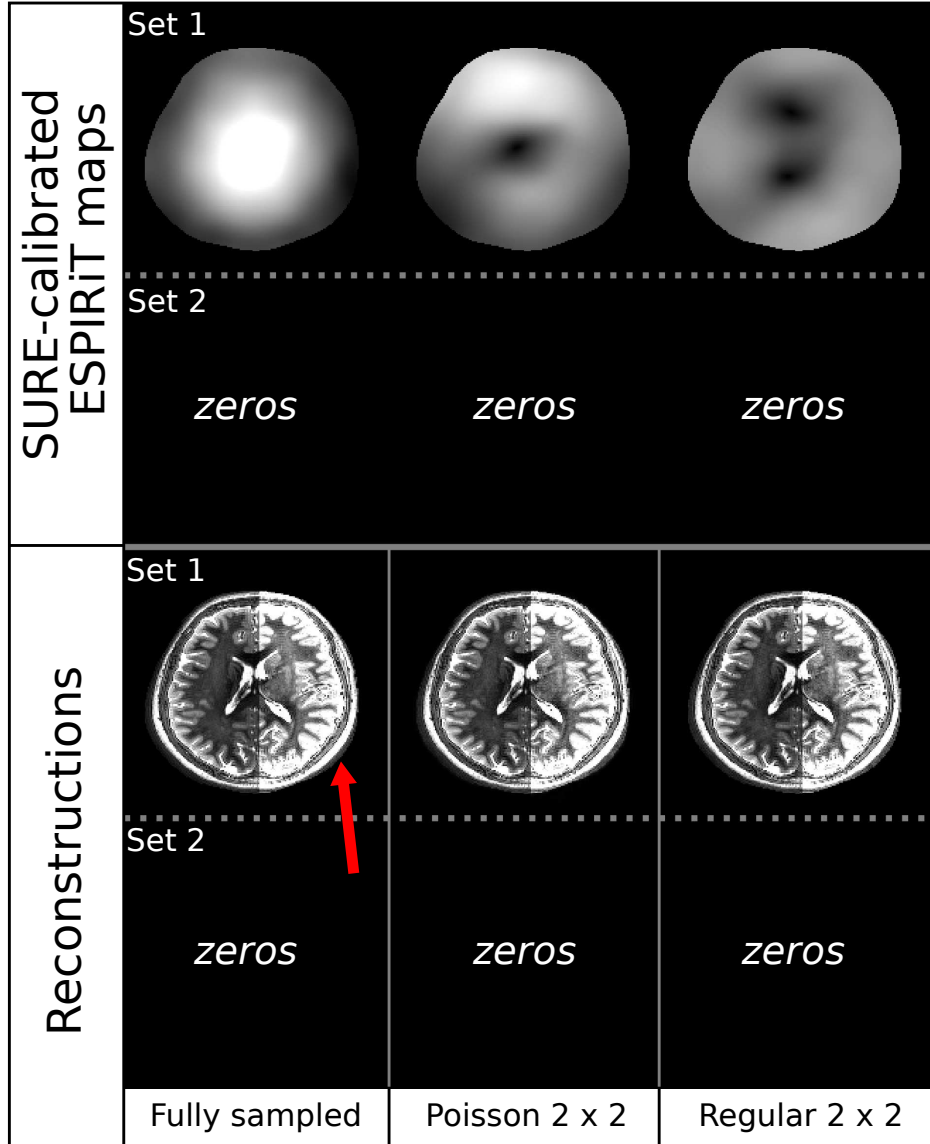


Figure 6: Experiment (g): This figure demonstrates the application of SURE to calibrate ESPIRiT maps on a T_2 -weighted acquisition. The ESPIRiT maps were calibrated using an ACS size of 18×18 after geometric coil compression. These were then used to reconstruct fully sampled k-space, 2×2 retrospectively under-sampled k-space using a Poisson mask, and 2×2 retrospectively under-sampled k-space using a regular equi-spaced 2×2 sampling mask. Half of the image’s contrast has been enhanced to illustrate how well the field of view of the desired object. “Set 1” and “Set 2” refers the “soft” SENSE model, where multiple ESPIRiT maps may satisfy the “ ≈ 1 ” eigenvalue condition. 3 for the 8 ESPIRiT maps are shown here for brevity.

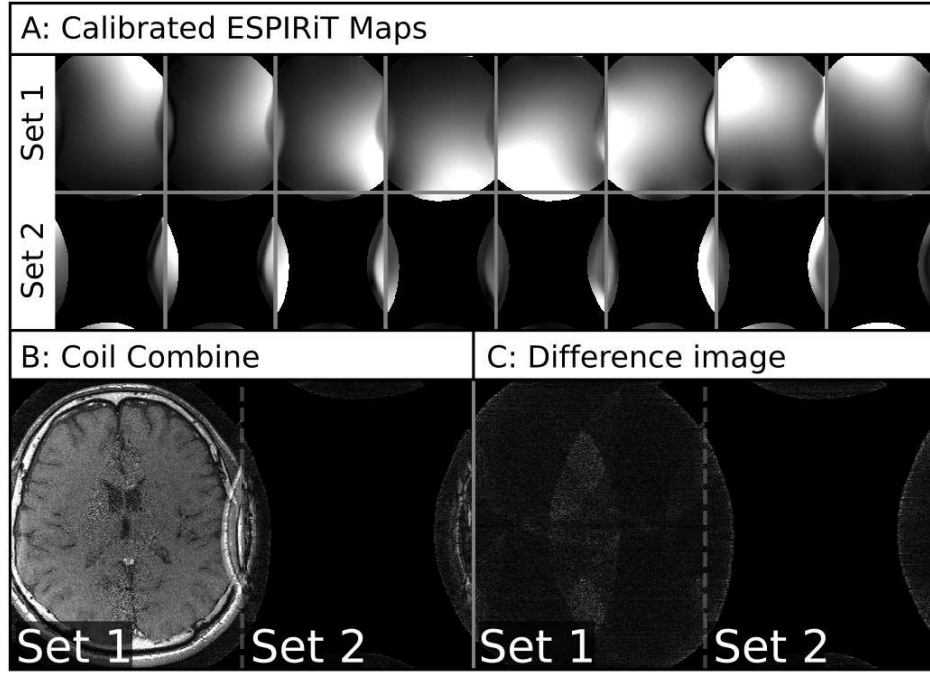


Figure 7: Experiment (h): Calibration With Aliasing Due To FOV Smaller Than Object Result. The data is retrospectively under-sampled using an equi-spaced 2×2 sampling mask with an ACS size of 24×24 . A fixed kernel size of 6 is used with the soft-threshold based subspace weighting heuristic. The eigenvalue crop threshold is varied. The data was Fourier transformed to the image domain and noise variance was estimated from a corner of the image data that did not contain any desired signal. Panel A shows the SURE-calibrated ESPIRiT maps, Panel B shows the 2×2 conjugate-gradient reconstruction and Panel C shows the difference between the fully sampled image and the 2×2 reconstructed image. It is seen that the SURE-based parameters selections results in parameters that retain ESPIRiT’s robustness to image aliasing.

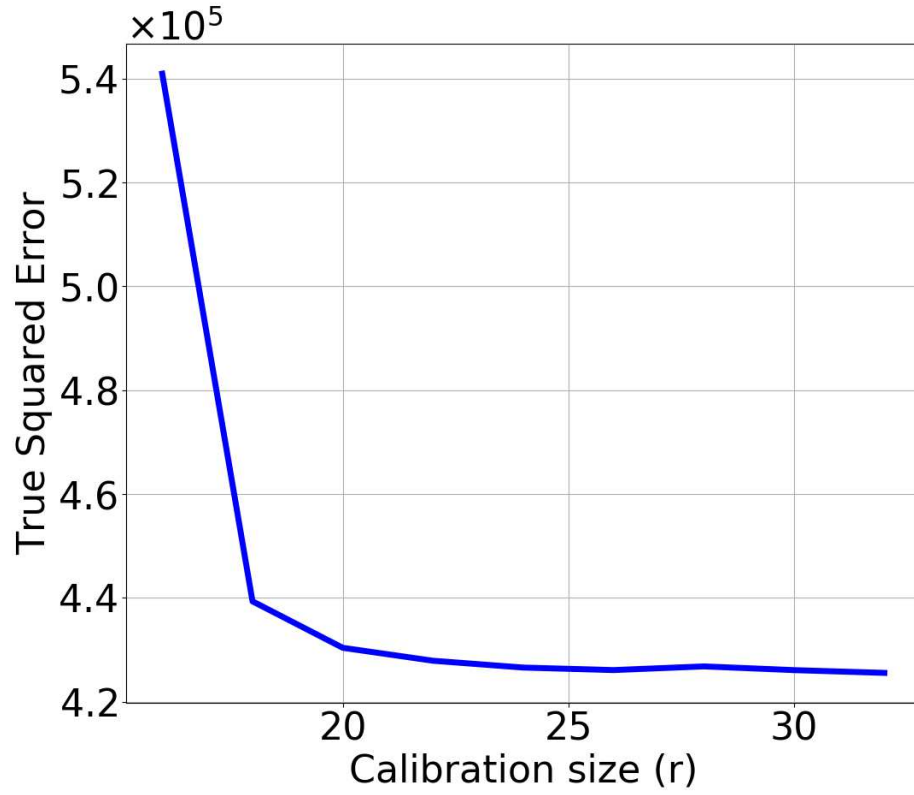


Figure 8: Experiment (i): This figure shows the effect of calibration size on the performance of ESPIRiT maps for a fixed kernel size ($k = 8$) and optimized crop threshold (c) assuming the soft-weighting heuristic. A calibration size of (r) implies $(r \times r)$ ACS lines. While a larger calibration size does result in a lower squared error, the advantage is on the order of 10^5 , which is much smaller than optimizing other parameters as in Experiments (a), (b), (c), and (d), which are on the order of 10^7 .

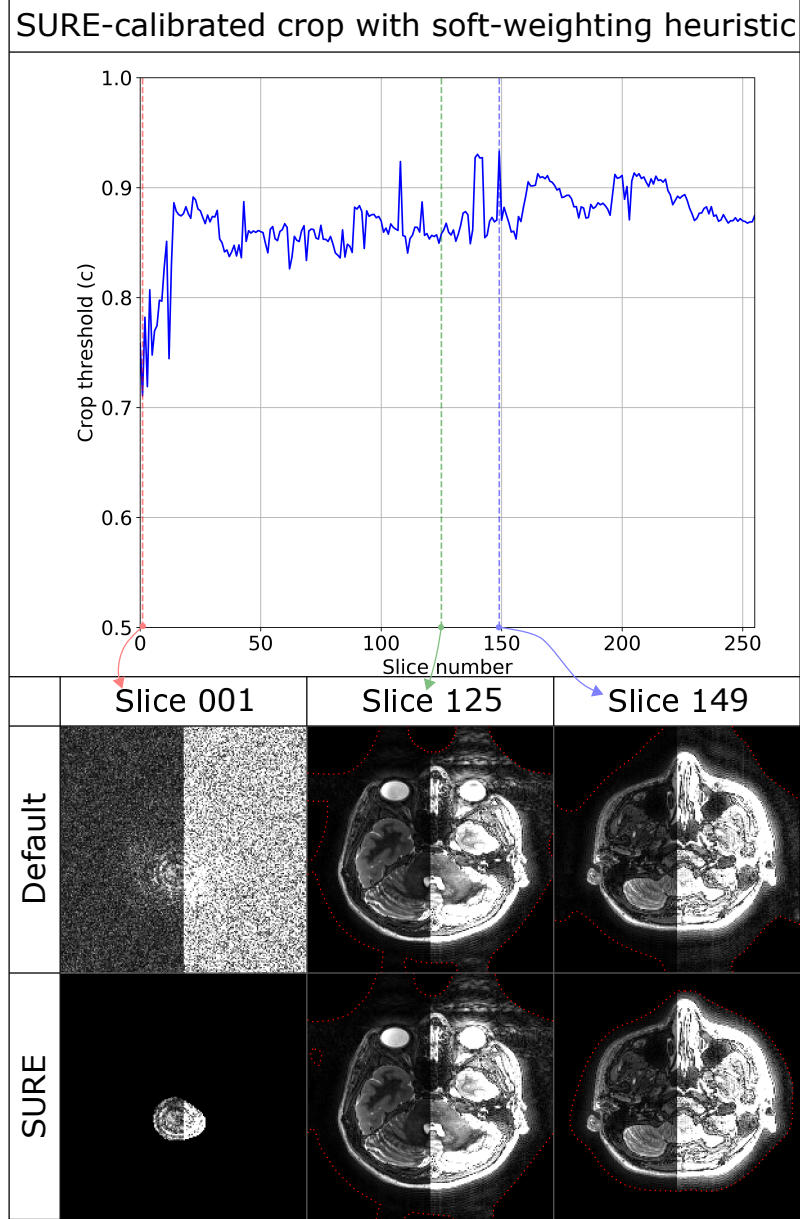


Figure 9: Experiment (j): SURE-optimal crop threshold per readout slice. If the readout direction is fully-sampled, an inverse Fourier transform can be taken and SURE+ESPIRiT can be applied to each readout slice. This will allow for ESPIRiT’s parameters to vary as a function of noise level per slice. The SURE-calibration used the soft-weighting heuristic. The default parameters correspond to a kernel size of 6 and a WNSVN corresponding to the number of singular values greater than 0.001 times the highest singular value. Since SURE tries to avoid data attenuation at all costs, the eye-motion related artifacts in Slice 125 results in spurious signal outside the human body. In contrast, the lack of motion in Slice 1 allows SURE to very finely calibrate ESPIRiT’s support about the FOV of the desired signal. The red dotted lines depict the FOV of the calibrated sensitivity maps.

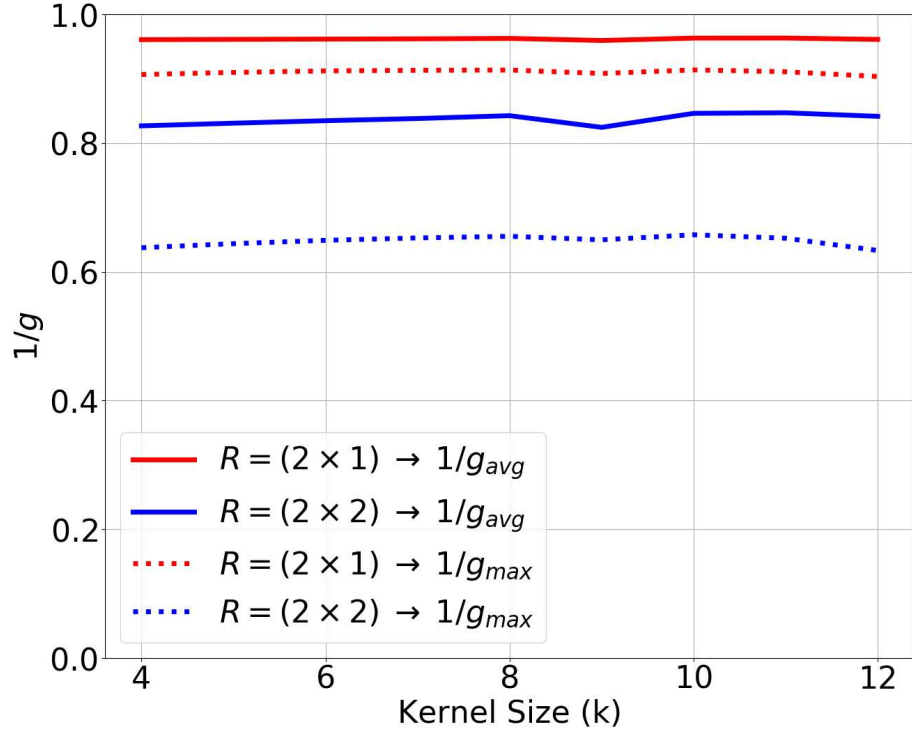


Figure 10: Experiment (k): This figure shows the effect of kernel size on the performance of ESPIRiT maps for assuming SURE-optimized crop threshold (c) and the soft-weighting heuristic. The calibration as performed on the same dataset as in Experiments (a), (b), (c) and (d). $R = 2 \times 1$ implies equispaced 2×2 under-sampling in both phase encode directions, while $R = 2 \times 1$ implies equispaced $2 \times$ under-sampling in one phase encode direction. It is seen that, when using an 8-channel coil, g-factor performance appears to be fairly stable as a function of kernel size.

List of Figures

1. Variability in ESPIRiT maps is exemplified by varying the signal subspace size (w) in WNSVN and eigenvalue crop threshold (c). These parameters are explained in the theory section. The mean g-factor g_{avg} and maximum g-factor g_{max} within the field of view of the desired object is used to quantify the performance of the ESPIRiT maps. $1/g_{\text{avg}}$ and $1/g_{\text{max}}$ are listed at top and bottom of the g-factor maps respectively. The g-factor is calculated assuming equispaced 2×2 sub-sampling in the phase encode directions. ESPIRiT maps that do not attenuate signal but have a high $1/g_{\text{avg}}$ and $1/g_{\text{max}}$ are desirable. Light pink mark regions of signal attenuation. In this figure, the best example is marked with a green box.
2. This summarizes the technique of generating ESPIRiT maps that are used as SENSE-like projection operators. (a) A kernel is swept through the calibration region to construct the calibration matrix (which consequently has block Hankel structure). (b) The SVD of the calibration matrix is taken and (c) the right singular vectors corresponding to the largest singular values are reshaped into k-space kernels. (d) The inverse Fourier transform of these kernels are taken, followed by (e) the eigenvalue decomposition of each pixel along the coil dimension in the image domain. The eigenvectors corresponding to eigenvalues “ ≈ 1 ” are used to construct the ESPIRiT operator. (f) depicts how ESPIRiT maps can be used as a projection operator to denoise data in the ideal case. (g) Consequently, the null space of the ideal projection operator would contain only noise.
3. Experiment (a): with a fixed kernel size of 6, the true squared error, SURE given densely-sampled, high-resolution data and normalized SURE given ACS data is calculated as a function of subspace size and eigenvalue crop threshold. The purple crosses show the locations of the respective minimum values. Experiment (b): with a fixed kernel size of 6 along with the soft-threshold based subspace weighting heuristic, the true squared error, SURE given densely-sampled, high-resolution data and normalized SURE given ACS data is calculated as a function of the eigenvalue crop threshold. Experiment (c): True squared error, SURE given densely-sampled, high-resolution data and normalized SURE given ACS data is calculated as kernel size, subspace size and eigenvalue crop threshold parameters are varied. The minimum given a particular kernel size is taken. Experiment (d) is similar to Experiment (c), except that instead of calculating the optimal subspace size given the kernel size, the soft-threshold based subspace weighting heuristic is used.
4. This figure shows how g-factor performance varies as a function of the Crop Threshold (c) when using the soft-weighting heuristic. The g-factor was calculated for voxels within the field of view of the brain using the same 2×2 equi-spaced sampling pattern described in Figure 1. Note that for all values of

(c) to the left of the green line (marked B), an increase in (c) results in a decrease in squared error as well as better g-factor performance. However, for values of (c) to the right of B , the resulting maps attenuate the desired signal. This is reflected by the increase in squared error. The purple line A reflects a safe value of the crop threshold, B reflects the optimal value in terms of minimum squared error and C represents the best g-factor but at the cost of a lot of signal attenuation. The optimality of B is also reflected in how well the field of view of the desired signal is captured. Half of the image’s contrast has been enhanced to illustrate this point.

5. Experiment (f): This figure demonstrates the application of SURE to calibrate ESPIRiT maps on a T_1 -weighted acquisition where roughly 50% of the total phase encode points are acquired, which included an ACS size of 18×18 . Half of the image’s contrast has been enhanced to illustrate how well the field of view of the desired object has been captured. “Set 1” and “Set 2” refers the “soft” SENSE model, where multiple ESPIRiT maps may satisfy the “ ≈ 1 ” eigenvalue condition. 2 of the 8 calibrated ESPIRiT maps are depicted in this figure for brevity.
6. Experiment (g): This figure demonstrates the application of SURE to calibrate ESPIRiT maps on a T_2 -weighted acquisition. The ESPIRiT maps were calibrated using an ACS size of 18×18 after geometric coil compression. These were then used to reconstruct fully sampled k-space, 2×2 retrospectively under-sampled k-space using a Poisson mask, and 2×2 retrospectively under-sampled k-space using a regular equispaced 2×2 sampling mask. Half of the image’s contrast has been enhanced to illustrate how well the field of view of the desired object. “Set 1” and “Set 2” refers the “soft” SENSE model, where multiple ESPIRiT maps may satisfy the “ ≈ 1 ” eigenvalue condition. 3 for the 8 ESPIRiT maps are shown here for brevity.
7. Experiment (h): Calibration With Aliasing Due To FOV Smaller Than Object Result. The data is retrospectively under-sampled using an equi-spaced 2×2 sampling mask with an ACS size of 24×24 . A fixed kernel size of 6 is used with the soft-threshold based subspace weighting heuristic. The eigenvalue crop threshold is varied. The data was Fourier transformed to the image domain and noise variance was estimated from a corner of the image data that did not contain any desired signal. Panel A shows the SURE-calibrated ESPIRiT maps, Panel B shows the 2×2 conjugate-gradient reconstruction and Panel C shows the difference between the fully sampled image and the 2×2 reconstructed image. It is seen that the SURE-based parameters selections results in parameters that retain ESPIRiT’s robustness to image aliasing.
8. Experiment (i): This figure shows the effect of calibration size on the performance of ESPIRiT maps for a fixed kernel size ($k = 8$) and optimized crop threshold (c) assuming the soft-weighting heuristic. A calibration size of (r) implies ($r \times r$) ACS lines. While a larger calibration size does result in a

lower squared error, the advantage is on the order of 10^5 , which is much smaller than optimizing other parameters as in Experiments (a), (b), (c), and (d), which are on the order of 10^7 .

9. Experiment (j): SURE-optimal crop threshold per readout slice. If the readout direction is fully-sampled, an inverse Fourier transform can be taken and SURE+ESPIRiT can be applied to each readout slice. This will allow for ESPIRiT's parameters to vary as a function of noise level per slice. The SURE-calibration used the soft-weighting heuristic. The default parameters correspond to a kernel size of 6 and a WNSVN corresponding to the number of singular values greater than 0.001 times the highest singular value. Since SURE tries to avoid data attenuation at all costs, the eye-motion related artifacts in Slice 125 results in spurious signal outside the human body. In contrast, the lack of motion in Slice 1 allows SURE to very finely calibrate ESPIRiT's support about the FOV of the desired signal. The red dotted lines depict the FOV of the calibrated sensitivity maps.
10. Experiment (k): This figure shows the effect of kernel size on the performance of ESPIRiT maps for assuming SURE-optimized crop threshold (c) and the soft-weighting heuristic. The calibration as performed on the same dataset as in Experiments (a), (b), (c) and (d). $R = 2 \times 1$ implies equispaced 2×2 under-sampling in both phase encode directions, while $R = 2 \times 1$ implies equispaced $2 \times$ under-sampling in one phase encode direction. It is seen that, when using an 8-channel coil, g-factor performance appears to be fairly stable as a function of kernel size.